Archives of Biochemistry and Biophysics 496 (2010) 84–92

Contents lists available at ScienceDirect

Archives of Biochemistry and Biophysics

journal homepage: www.elsevier.com/locate/yabbi

Size-dependent neurotoxicity of β-amyloid oligomers

Paulius Cizas [a,b,1], Rima Budvytyte [c,1], Ramune Morkuniene [a,b], Radu Moldovan [d], Matteo Broccio [d], Mathias Lösche [d], Gediminas Niaura [c], Gintaras Valincius [c], Vilmante Borutaite [a,*]

[a] Institute for Biomedical Research, Kaunas University of Medicine, Kaunas, Lithuania
[b] Department of Biochemistry, Kaunas University of Medicine, Kaunas, Lithuania
[c] Institute of Biochemistry, Vilnius, Lithuania
[d] Department of Physics, Carnegie Mellon University, Pittsburgh, USA

ARTICLE INFO

Article history:
Received 10 November 2009
and in revised form 4 February 2010
Available online 11 February 2010

Keywords:
Beta amyloid
Oligomers
Fibrils
Neurons
Cell death
Atomic force microscopy
Dynamic light scattering
Fluorescence correlation spectroscopy

ABSTRACT

The link between the size of soluble amyloid β(Aβ) oligomers and their toxicity to rat cerebellar granule cells (CGC) was investigated. Variation in conditions during *in vitro* oligomerization of $A\beta_{1-42}$ resulted in peptide assemblies with different particle size as measured by atomic force microscopy and confirmed by dynamic light scattering and fluorescence correlation spectroscopy. Small oligomers of $A\beta_{1-42}$ with a mean particle *z*-height of 1–2 nm exhibited propensity to bind to phospholipid vesicles and they were the most toxic species that induced rapid neuronal necrosis at submicromolar concentrations whereas the bigger aggregates (*z*-height above 4–5 nm) did not bind vesicles and did not cause detectable neuronal death. A similar neurotoxic pattern was also observed in primary cultures of cortex neurons whereas $A\beta_{1-42}$ oligomers, monomers and fibrils were non-toxic to glial cells in CGC cultures or macrophage J774 cells. However, both oligomeric forms of $A\beta_{1-42}$ induced reduction of neuronal cell densities in the CGC cultures.

Introduction

The central event in pathogenesis of Alzheimer's disease (AD)[2] is thought to be intracellular and extracellular accumulation of polypeptide compounds of low molecular mass – so called beta amyloid (Aβ). These molecules tend to aggregate and form complexes of varying size: from small soluble oligomers, bigger protofibrils and finally insoluble fibrils. It is commonly assumed that formation of Aβ fibrils and plaque deposits is a crucial event in the pathogenesis of AD [1]. However, there is accumulating evidence that soluble oligomers are the most cytotoxic form of Aβ although it is still unclear which size and morphology of the aggregates exert neurotoxicity. The level of soluble forms of Aβ was shown to strongly correlate with the severity of the disease [2,3]. In addition, it has been shown that soluble oligomeric Aβ species are responsible for a decrease in the long-term potentiation and disruption of synaptic plasticity in AD affected neurons [4–7]. Electrophysiological studies demonstrated that a trimeric form of $A\beta_{1-42}$ inhibits long-term potentiation in rodents most effectively [8]. Furthermore, it has been reported [9] that freshly prepared $A\beta_{1-42}$ oligomers rapidly induce endoplasmic reticulum stress which results in activation of caspases and apoptosis of cortical neurons in culture, whereas aged fibrillar preparations of $A\beta_{1-42}$ were much less toxic to neurons. Notably, it has been demonstrated that $A\beta_{1-42}$ tends to form thermodynamically stable trimeric and tetrameric forms that are not obligatory intermediates in the amyloid fibril formation pathways [2]. On the other hand, spherical oligomeric particles with molecular weights ranging from 90 to 110 kDa (diameters in the range of 3–5 nm) were shown to drastically increase the permeabilization of lipid bilayers [10] which is possibly related to the observed neurotoxicity. Even though distinct differences in the cytotoxicity of very large fibrillar assemblies and small soluble oligomers are now a well established fact [11], there is some experimental evidence that the neurotoxicity may differ significantly even within amyloid aggregate populations with relatively small molecular weights [12]. The purpose of the present work was to establish and quantify the dependence of neurotoxic effects on the size of synthetic $A\beta_{1-42}$ oligomers with molecular weights below ~100 kDa.

Materials and methods

The procedures used in this study are approved by the European Convention for the protection of vertebrate animals used for

* Corresponding author. Address: Institute for Biomedical Research, Kaunas University of Medicine, Eiveniu str. 4, Kaunas LT-50009, Lithuania. Fax: +370 37 302959.
E-mail addresses: vilbor@vector.kmu.lt, vilbor@gmail.com (V. Borutaite).

[1] These authors contributed equally to this work.

[2] *Abbreviations used:* Aβ, beta amyloid; AD, Alzheimer's disease; AFM, atomic force microscopy; araC, cytosine arabinoside; CD, circular dichroism; CGC, cerebellar granule cells; Chol, cholesterol; DIV, days *in vitro*; DLS, dynamic light scattering; DOPC, dioleoylphosphatidylcholin; DOPS, dioleoylphosphatidylserine; FCS, fluorescence correlation spectroscopy; FTIR, Fourier transform infrared spectroscopy; HFIP, hexafluoroisopropanol; LDH, lactate dehydrogenase; PI, propidium iodide.

0003-9861/$ - see front matter © 2010 Elsevier Inc. All rights reserved.
doi:10.1016/j.abb.2010.02.001

experimental and other purposes and according to the Republic of Lithuania law on the care, keeping and use of animals.

Neuronal-glial culture preparation

Mixed neuronal-glial CGCs cultures were prepared from 7 to 8 day old Wistar rats as described [13]. Cells were grown *in vitro* for 5–6 days before exposure to Aβ. The cultures contained 1.8 ± 0.5% microglial cells, as assessed by staining with isolectin GS-IB4, and 7.3 ± 4.9% astrocytes, as assessed by cellular morphology.

Preparation of Aβ monomers, oligomers and fibrils

Synthetic $A\beta_{1-42}$ peptide was from Bachem (Switzerland) and American Peptide (California, USA). HiLyte Fluor™ 555 labeled $A\beta_{1-42}$ peptide was from Anaspec (California, USA). Oligomers were generated as described [14,15]. Briefly, soluble oligomers were prepared by dissolving 1 mg of peptide in 400 μl HFIP for 30–60 min at room temperature. Sonication was used in this step. About 100 μl of the resulting seedless solution was added to 900 μl H_2O in a siliconized Eppendorf tube. After 10–20 min incubation at room temperature, the samples were centrifuged for 15 min at 12,000 rpm, the supernatant was transferred to a new siliconized tube and HFIP was evaporated. Concentration of HFIP in solution was monitored in FTIR spectra by a decrease in intensity of the 1192 cm^{-1} band due to the asymmetric CF_3 stretching vibration [16] (see Supplemental material, Figs. S1 and S2). Samples were incubated in closed vials for 24 h at 20 °C. This protocol is denoted as *protocol I*. FTIR spectroscopy showed also that the usage of siliconized centrifuge tubes, essential to produce fractions of oligomeric particles with sizes below 3 nm, resulted in transfer of some of the silicon oil components into the vials, which caused strong absorption bands near 1261 and 2962 cm^{-1}, assigned to the bending and stretching vibrations of $Si–CH_3$ and CH_3 groups, respectively. Vehicle was prepared in the same way as oligomeric forms but without $A\beta_{1-42}$ (thus containing similar amounts of residual HFIF or silicone oil). To generate larger oligomers, typically 4–10 nm in diameter, the supernatant was transferred to a non-siliconized Eppendorf tube after the centrifugation and was gently purged with nitrogen for 7 min. The preparation was then stirred in the same vial at ~500 rpm for 24 h using a magnetic Teflon-coated stirring bar. Such a protocol will be further referred to as *protocol II*. Fibrils were formed by *protocol III* in which the aqueous peptide solution obtained after evaporation of HFIP was incubated for 7 days at room temperature. Monomers were prepared by dissolving $A\beta_{1-42}$ in HFIP and, after removal of HFIP by evaporation, resuspending in DMSO at a concentration of 0.5 mM. All samples were centrifuged for 15 min at 12,000 rpm and the supernatant was transferred to a new siliconized tube. Solutions of peptides were stored at −20 °C.

Fractionation of $A\beta_{1-42}$ preparations

Ultrafiltrations of $A\beta_{1-42}$ preparations were performed using Microcon YM-10, YM-30 and YM-100 filters (Millipore) according to manufacturer's instructions. Briefly, the solutions of freshly prepared $A\beta_{1-42}$ oligomers were filtrated through Microcon filter with cut-off at 100 kDa for 12 min at 12,000*g*. The resulting retentate was supplemented with 100 μl H_2O and recovered by reverse spinning to obtain the fraction with weight of >100 kDa. The supernatant of the first filtration was centrifuged either through the 30 kDa filter (12 min at 12,000*g*) to obtain as the supernatant the fraction with weights of <30 kDa or through the 10 kDa filter (30 min at 12,000*g*) to obtain as the supernatant the fraction with weights of <10 kDa. The retentate after filtration through 30 kDa filter was recovered by reverse spinning (plus 100 μl H_2O) and used as the fraction with weights >30 kDa. Protein concentration in the samples was determined by the Bradford method.

Characterization of oligomer preparations

To assess the size and morphology of the preparations of $A\beta_{1-42}$ oligomers and fibrils, atomic force microscopy (AFM; Agilent 5500, Santa Clara, CA) was used in the tapping mode. Model TESP (Veeco, Plainview, NY) (f = 257–301 kHz, k = 20–80 N/m) and model PPP-NCL-20 (f = 146–236 kHz, k = 21–98 N/m) (Nanosensors, Neuchatel, Switzerland) microcantilevers were used in this work. According to the manufacturers, the probe tip diameters were between 16 and 20 nm. About 20 μl of a 10 μM $A\beta_{1-42}$ solution was spotted on freshly cleaved mica (SPI Supplies, West Chester, PA), incubated at room temperature for 10 min and rinsed with deionized water (Millipore Inc.), then blown dry with a nitrogen stream. Images were acquired at scan rates between 0.5 and 1 Hz with the drive amplitude and force kept to a minimum. The particle size was estimated by measuring the profile of the sample within the sample plane. The mean height of amyloid aggregates ("z-height") was estimated by using the Plane Correction (Flattening) module of the SPIP software and determining step-height histograms.

Dynamic light scattering (DLS) experiments were performed on a Zetasizer Nano ZS (Malvern Instruments Ltd., UK) using a laser source with λ = 633 nm and a detector at a scattering angle of θ = 173°. Relaxation time distributions were obtained numerically from the field autocorrelation function $g_1(t)$ by means of a regularized inverse Laplace transform routine. Particle size distributions were extracted from the latter through the Stokes–Einstein equation assuming spherical shapes of the particles.

Fluorescence correlation spectroscopy (FCS) was carried out on a Zeiss LSM 510 Meta equipped with a Confocor 3 detection module. Excitation light λ = 561 nm, provided by a diode-pumped solid state (DPSS) laser, is coupled into a 40 × 1.1 NA LD-C-Apochromat water immersion objective and the fluorescence emission is epi-collected through the same objective and detected by an avalanche photodiode mounted behind a 575–615 nm bandpass filter. FCS data were fitted with a 3D diffusion model [17] providing the oligomer diffusion coefficient which converts into oligomer size via the Stokes–Einstein equation. Concerning corrections for non-spherical aggregate shares, see Supplemental material. A small fraction (0.2 mol%) of fluorescently labeled $A\beta_{1-42}$ peptide was used in FCS experiments probing size distribution.

CD spectra were collected on a Jasco J-810 spectropolarimeter. Spectra were obtained from 185 to 270 nm with a resolution of 0.2 nm and a bandwidth of 1 nm in a 1-cm path length quartz cell. Spectra were then converted to mean residue ellipticity and data were analyzed by using CDPro.

FTIR measurements were performed on a Perkin-Elmer model Spectrum GX FTIR spectrometer equipped with a DTGS detector. FTIR spectra were recorded in transmission mode. The spectral resolution was set to 2 cm^{-1} and spectra were acquired by co-adding 50 scans. HFIP solution spectra were recorded in a sealed cell with 25 μm path length equipped with CaF_2 windows. $A\beta_{1-42}$ preparations were deposited on CaF_2 substrate from 60 μM solution and were dried in air.

Details of the MALDI-TOF characterization of peptide oligomers are given in the Supplemental materials.

Assessment of cell viability

The viability of neuronal cells in the cultures treated for 24 h with $A\beta_{1-42}$ or vehicle (control) was assessed by propidium iodide (PI, 7 μM) and Hoechst 33342 (4 μg/ml) staining using a fluorescence microscope OLYMPUS IX71S1F-3. PI-negative cells with

weak Hoechst staining were considered to be viable, whereas cells showing nuclear shrinkage or fragmentation and intensive Hoechst staining, but still lacking PI staining, were classified as chromatin condensed/fragmented (apoptotic). PI-positive cells were classified as necrotic. Neuronal cells were distinguished from glial cells according to their characteristic shape and nuclear morphology. Microglial cells were additionally identified by using Isolectin GS-IB4 conjugated with AlexaFluor488 (7 ng/ml, Invitrogen). Neuronal cells were counted in at least five microscopic fields per well (two wells per treatment) and expressed as a percentage of the total number of neuronal cells per field.

The activity of lactate dehydrogenase (LDH) released into the medium (an indicator of necrosis) was measured spectrophotometrically [18] by monitoring decrease in NADH at 340 nm as pyruvate is converted to lactate (200 μl aliquot of medium taken from cell culture was added to 0.1 M Tris–HCl buffer, pH 7.5, containing 0.1 mM NADH and 1 mM Na–pyruvate). LDH activity in control groups was equated to 100%.

Vesicle preparation

Vesicles were prepared by mixing stock lipid solutions (10 mg/ml) in chloroform at the ratio, DOPC/DOPS/Chol = 63:7:30, in a glass tube. Lipid ratios were chosen to mimic to a first approximation neuron membrane composition [19]. 1 ml of lipid mixture was evaporated by a gentle stream of N_2. The residual solvent was removed by vacuum-drying the lipid film for 1 h. The film then was dissolved in pentane (1 ml) and left to dry overnight in the hood. The film was hydrated by adding 2.5 ml of working buffer, 100 mM NaCl, NaH_2PO_4 (pH 7.4), sonicating for 60 min and incubating with occasional vortexing or until the lipid film at the bottom disappeared. The lipid preparation was then extruded (Avanti Polar Lipids, USA) through a 100 nm polycarbonate membrane for 21 times. Size distribution of vesicles was determined by dynamic light scattering. The preparation exhibited a single peak centered around 150 nm (see Supplemental material). A large excess of vesicles was used in the oligomer binding to phospholipid experiments. The amyloid (monomer) concentration used in binding to vesicles experiment was 2.8 M, of which 10% was labeled with Hi-Lyte Fluor™ 555. Binding experiments were carried out in 5× diluted vesicle solutions with 2 mg/ml total lipid concentration.

Statistical analysis

Data are expressed as mean ± SE of 3–7 experiments on separate CGC cultures. Statistical comparison between experimental groups was performed using Student's *t*-test. Pearson's correlation method (r) with 99% confidence interval was used for correlation analysis.

Results

We analyzed the effect of various $A\beta_{1-42}$ assemblies on the viability of CGCs. As shown in Fig. 1A, treatment of cells with $A\beta_{1-42}$ oligomers prepared by *protocol I* caused a gradual decrease of neuronal viability in a concentration dependent manner: 94% viability in controls decreased to 11% at 2 μM $A\beta_{1-42}$. In contrast, $A\beta_{1-42}$ fibrils and monomers had no effect on neuronal viability even at 2 μM concentrations. Vehicle had no effect on cell viability. $A\beta_{1-42}$ induced cell death was mainly necrotic as the percentage of PI-positive cells was significantly elevated with the increase of $A\beta_{1-42}$ concentration (Fig. 1B). Measurement of LDH activity in the culture media confirmed this observation: the activity of LDH released from cells was found to increase gradually from 10% in cells treated with 0.5 μM to about 70% after treatment with 2 μM $A\beta_{1-42}$ oligomeric preparations (Fig. 1C). The percentage of apoptotic cells showing nuclear shrinkage and chromatin condensation was minor (5–10%) with all concentrations of $A\beta_{1-42}$ oligomers (Fig. 1B).

Importantly, $A\beta_{1-42}$ oligomers affected only neurons whereas glial cells were resistant to monomeric, oligomeric and fibrillar forms of the peptide (data not shown). In addition, we tested the effect of $A\beta_{1-42}$ oligomers on the murine macrophage J774 cell line and found that at 1 μM concentration $A\beta_{1-42}$ oligomers prepared by *protocol I* did not cause cell death: viability of J774 cells after 24 h incubation with $A\beta_{1-42}$ was 96.5 ± 0.6% compared to 97.0 ± 0.3% in cells treated with vehicle. Neither $A\beta_{1-42}$ monomers nor fibrils were toxic to J774 cells (data not shown).

To determine whether the toxicity of $A\beta_{1-42}$ peptides is CGC neuron specific, we performed experiments comparing the effects of various $A\beta_{1-42}$ preparations on primary culture of cortical neurons. We found that cortical neurons responded to $A\beta_{1-42}$ in a similar manner as CGCs: 1 μM $A\beta_{1-42}$ oligomers prepared by *protocol I* caused a decrease of neuronal viability by 40% compared to viability of control cultures after 24 h incubation, whereas $A\beta_{1-42}$ monomers and fibrils had no effect on viability of cortical neurons (see Supplemental Fig. S5). This indicates that neurons isolated from different parts of the brain are similarly sensitive to $A\beta_{1-42}$ oligomers and insensitive to fibrillar and monomeric forms of $A\beta_{1-42}$ at least during a short time (24 h) of exposure.

In contrast to $A\beta_{1-42}$ oligomers prepared by *protocol I*, oligomers prepared by *protocol II* were not toxic to CGC cultures. We then questioned whether the two protocols may generate $A\beta_{1-42}$ oligomeric particles of different sizes and thus influence the cytotoxicity of preparations. To investigate this possibility, we carried out an AFM analysis of various $A\beta_{1-42}$ preparations precipitated on freshly cleaved mica. Typical results are shown in Fig. 2A–C. Evidently, not only the morphology (oligomers vs. fibrils) but also a size of soluble oligomers depends on the preparation protocol. Analysis of AFM images shows that oligomers prepared by *protocol I* exhibited mean z-height values spanning from 1 to 3 nm (Fig. 2A and D), in few cases reaching 4–5 nm. In distinction, *protocol II* yielded considerably larger rounded species with sizes of 5–10 nm. The lateral size of the oligomers in AFM images, however, is significantly larger. For the smallest particles with a mean z-height of 1.41 ± 0.06 nm (33 counts), the average lateral size of the particle image was 39.8 ± 2.7 nm (30 counts). The lateral size correlated with the z-height of the particles linearly as $r_{xy} = 7z + 26$ nm ($R^2 = 0.8$), where r_{xy} and z are the lateral size and z-height of a particle in nm, respectively. The coefficients in the equation varied by up to 45% depending on the direction along which the image was recorded. This may reflect an asymmetry of the imaging tip.

To investigate how drying of the peptide sample for AFM investigation affects aggregate sizes we carried out DLS and FCS measurements in solutions containing different forms of $A\beta_{1-42}$ oligomers. Both methods confirm that *protocol I* typically generates particles with sizes from 1 to 4 nm. Representative particle size distributions obtained with DLS are shown in Fig. 3A. Preparations obtained via *protocols I* (light gray) and *II* (dark gray) differ significantly. In this particular data set, *protocol I* oligomers show an average diameter of ~2.7 nm, while the *protocol II* particles had average diameter of ~8 nm (assuming spherical particle shape). This result is consistent with the AFM data and suggests that drying for AFM imaging does not significantly alter particle size. FCS data obtained with fluorescently labeled aggregates indicated similar particle size distributions, which, in case of *protocol I* preparations (Fig. 3B) exhibits two maxima: one with the mean diameter at ~3.4 nm and another with smaller intensity at ~8 nm. MALDI-TOF mass spectra (see Supporting material, Fig. S3) show oligomer species with molecular weights up to ~22.54 kDa in preparations obtained by *protocol I*, while molecular weights of up to

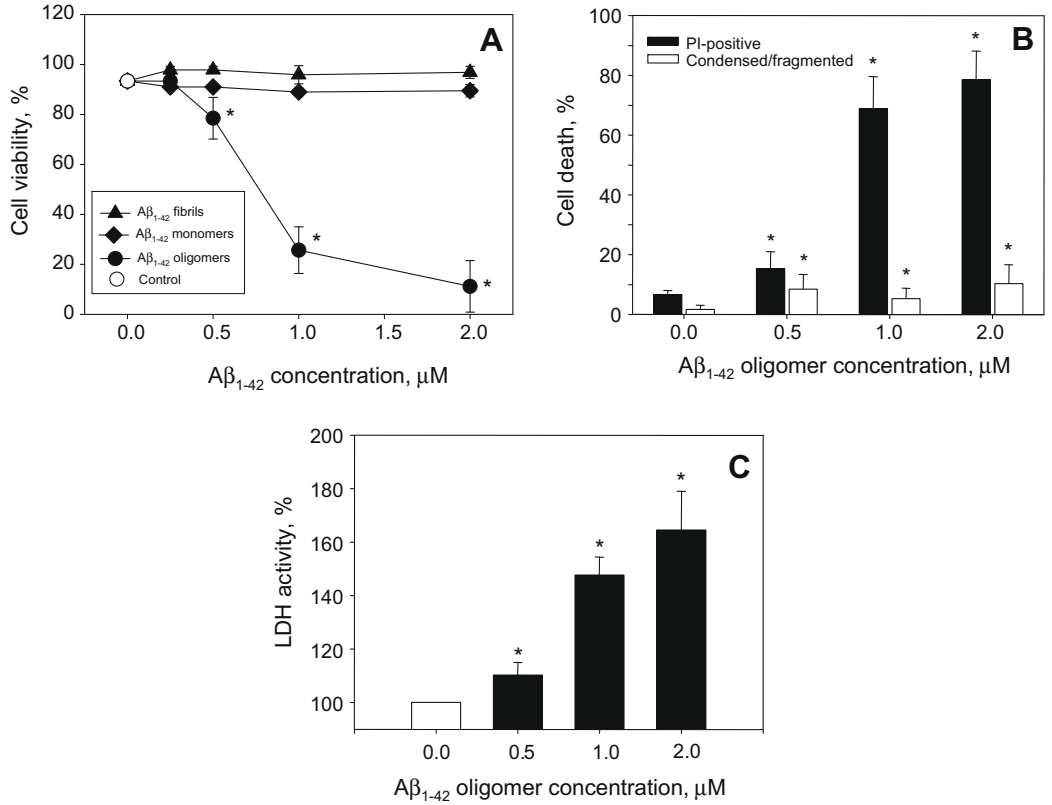

Fig. 1. Effect of differently prepared $A\beta_{1-42}$ assemblies on neuronal cell viability in CGC cultures. (A) Effect of $A\beta_{1-42}$ oligomers (*protocol I*), fibrils (*protocol III*) and monomers on neuronal cell viability; (B) concentration dependence of $A\beta_{1-42}$ oligomers (*protocol I*) to induce necrotic (PI-positive) and apoptotic (condensed/fragmented nuclei) cell death of neurons. (C) Effect of $A\beta_{1-42}$ oligomers (*protocol I*) on LDH release from cells into medium. LDH activity in the control group was equated to 100%. ∗ – statistically significant effect of Aβ if compared to control. Means ± standard errors of 5–7 experiments on separate CGC cultures are presented.

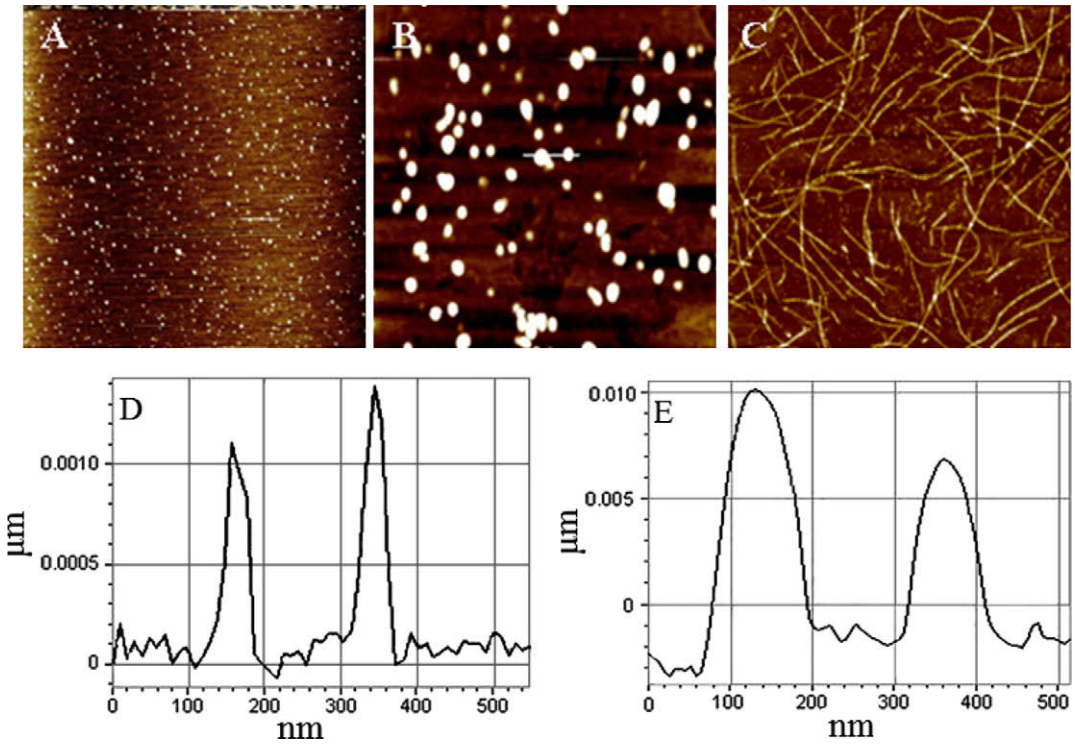

Fig. 2. AFM results. Exemplary images of $A\beta_{1-42}$ oligomers prepared by the different protocols: (A) *protocol I*, (B) *protocol II*, (C) *protocol III*. The lateral size of the images is 4×4 μm. The horizontal bars in A and B show the location at which height profiles of the images were analyzed. (D and E) are the corresponding cross-sections of the particles obtained via *protocols I* and *II*.

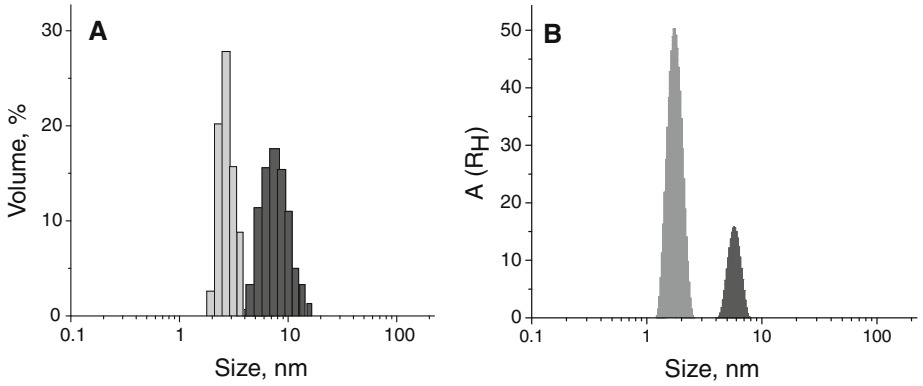

Fig. 3. Size distribution of differently prepared $A\beta_{1-42}$ oligomers. (A) DLS. Light gray: *protocol I* aggregates, dark gray: *protocol II* aggregates. The larger size oligomer preparation contained also a small contribution of sizes above 200 nm (not shown). (B) FCS results for *protocol I* and *II* oligomers with the same coding as in panel (A).

~45.16 kDa were detected in preparations obtained via *protocol II*. In all cases, preparations were polydisperse in AFM images (Fig. 2), DLS and FCS results (Fig. 3A and B).

The relationship between the toxicity of $A\beta_{1-42}$ oligomers and their size is presented in Fig. 4. At 1 μM concentration, small $A\beta_{1-42}$ particles (1–2 nm *z*-height in AFM) obtained by *protocol I* were highly toxic to neurons: after 24 h of incubation just 10–40% of viable neurons were observed. Toxicity of $A\beta_{1-42}$ decreased with increase in the size of the particles: 50–85% of viable cells were observed after incubation with medium-sized $A\beta_{1-42}$ particles (3–5 nm *z*-height, *protocols I* and *II*). Larger particles (5–9 nm *z*-height, *protocol II*) were non-toxic to neurons. This suggests that the neurotoxicity depends on $A\beta_{1-42}$ oligomer size (Pearson's correlation coefficient $r = 0.74$) rather than on the protocol by which the particles are generated, as small oligomers prepared by *protocol I* are the main cytotoxic species but larger particles prepared by either *protocols I* and *II* show comparably low cytotoxicity.

The toxic effects of Aβ oligomers may depend on the presence of functional NMDA receptors whose expression is delayed in CGC cultures and reaches a maximum on 10–12 DIV. To test this, we performed series of experiments investigating the effect of various forms of $A\beta_{1-42}$ on mature, 10–14 DIV CGC cultures. As can be seen in Fig. 5, the effects of $A\beta_{1-42}$ peptides were similar as on 5–6 DIV CGC: 1–2 nm oligomers of $A\beta_{1-42}$ at 1 μM concentration were the most toxic species to mature CGCs, decreasing neuronal viability by about 60% compared to control, whereas lager, 4–6 nm oligomers as well as monomers and fibrils were not toxic to mature CGC. $A\beta_{1-42}$-oligomer-induced neuronal death in mature cultures was mainly (about 60%) necrotic (Fig. 5).

For a refined analysis seeking to reduce the polydispersity of preparations shown in Fig. 3, we fractionated aggregate sizes by filtering to obtain oligomers with weight ranges of <10, 10–30, and >30 kDa (see Materials and methods). Fig. 6 shows the dependence of neurotoxicity on those fractionated amyloid preparations. Specifically, the exposure of CGCs to the fraction of $A\beta_{1-42}$ oligomers collected after filtering through the 30 kDa filter reduced neuronal survival by ~60% at 0.35 μM $A\beta_{1-42}$ concentration and to less than 10% at 1 μM concentration. Other fractions were not significantly toxic to CGCs.

Although the cytotoxicity of $A\beta_{1-42}$ oligomers of different sizes differs significantly, CD spectra do not show differences in their secondary structure (Table 1). The contributions of the secondary structure elements are undistinguishable in preparations obtained by *protocols I* and *II*. In contrast, distinctive differences in the distribution of secondary structure elements are observed in monomeric peptide. The content of α-helixes and β-sheet structures in the monomer preparation is higher than previously reported (53% and <1%, respectively) [20], presumably because of the sonication used in our work. FTIR spectra of $A\beta_{1-42}$ oligomers deposited on CaF_2 substrate revealed several subtle size-dependent differences

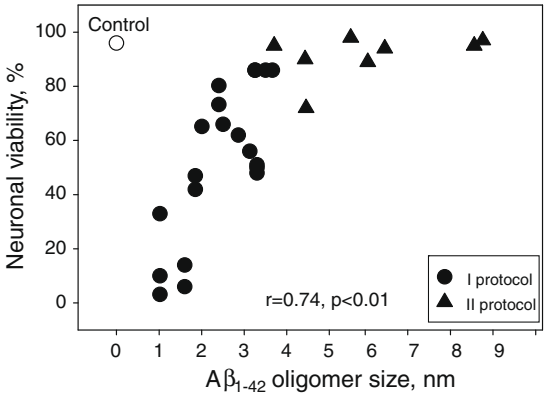

Fig. 4. Toxicity of $A\beta_{1-42}$ oligomers depends on aggregate size as determined with the AFM in terms of *z*-height. $A\beta_{1-42}$ oligomers were prepared by *protocols I* and *II*. CGCs were treated with 1 μM $A\beta_{1-42}$ oligomers for 24 h. Each point represents the effect of a separate preparation of oligomers on viability of separate CGC culture (mean values are presented for each experiment).

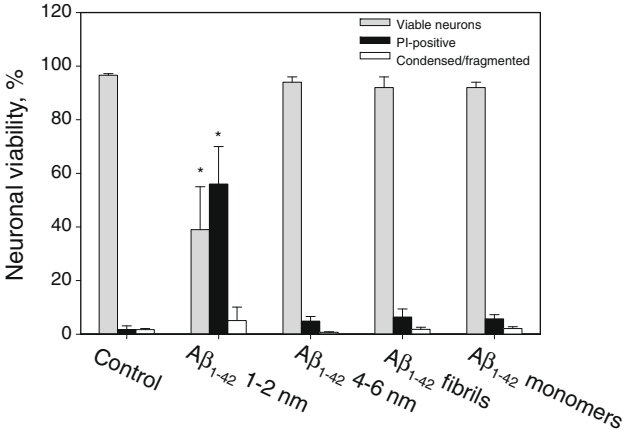

Fig. 5. Effect of $A\beta_{1-42}$ peptides on neuronal cell viability in 10–12 DIV CGC cultures. Mixed neuronal-glial CGCs cultures were prepared from 7 to 8 day old Wistar rats as described in Material and methods. Cells were grown *in vitro* for 10–14 days, then treated with 1 μM $A\beta_{1-42}$ peptide for 24 h. The viability of neurons in the culture was measured by propidium iodide and Hoechst 33342 staining. * – statistically significant effect of Aβ peptide, if compared to control. Means ± standard errors of four separate experiments are presented.

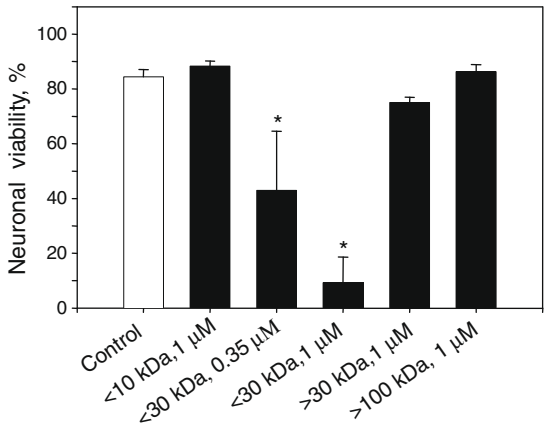

Fig. 6. Effect of $A\beta_{1-42}$ on neuronal viability depends on the molecular mass of the peptide assemblies. $A\beta_{1-42}$ oligomer preparations were fractionated through different Microcon filters as described in Materials and methods. * – statistically significant effect of Aβ if compared to control. Means ± standard errors of 3–6 separate experiments are presented.

Table 1
Distribution of secondary structure elements in $A\beta_{1-42}$ preparations as determined by the CD spectroscopy.

Peptide $A\beta_{1-42}$	α-Helix (%)	β-Sheet (%)	Turn (%)	Disordered (%)
$A\beta_{1-42}$ monomers	71	13	8	8
$A\beta_{1-42}$ small oligomers, *protocol I*	4	43	21	32
$A\beta_{1-42}$ larger oligomers, *protocol II*	4	43	21	32

in the Amide-I spectral region (Fig. 7). In agreement with the CD data, the β-sheet secondary structure motive (1628 cm^{-1} band) dominates for both small and larger oligomers. However, the difference spectrum shows larger absorbance of the small oligomers at 1616 and 1696 cm^{-1}. The absorbance increase near 1616 cm^{-1} indicates a shift of the 1628 cm^{-1} component to lower wavenumbers for small oligomers, possibly associated with a different organization of the β-sheet structure due to stronger hydrogen bonding, as strong intermolecular β-strand interaction has been shown to result in a low-frequency shift [21]. The high frequency component (1696 cm^{-1}) is associated with the same intermolecular β-sheet structure. The broad positive band near 1668 cm^{-1} may indicate the presence of relatively larger contents of loop, turn and α-helix structures in small oligomers [21].

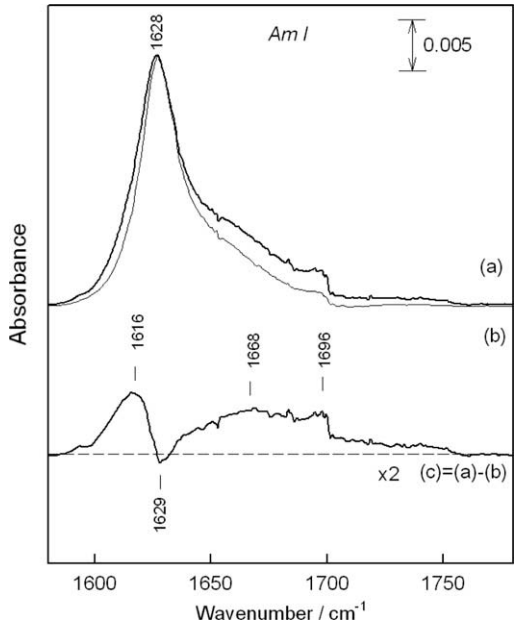

Fig. 7. $A\beta_{1-42}$ aggregate size causes FTIR spectral differences in the Amide-I spectral region. (a) Small oligomers (*protocol I*), (b) larger oligomers (*protocol II*), and (c) difference spectrum. Transmission spectra were obtained from dried samples deposited on CaF_2 substrates from 60 μM solutions.

To assess whether different size oligomer preparations bind differently to phospholipid membranes we carried out vesicle binding test using FCS. Fig. 8 shows FCS correlation curves fitted with appropriate 3D diffusion models for two different size oligomers preparations. The experiment sequence was as follows. First, we observed oligomers prepared via *protocols I* (Fig. 8A) and *II* (Fig. 8B) diffusing freely in solutions without vesicles (grey dots/red dots in on-line version). These data were fitted with a single component 3D diffusion model shown as red continuous lines, and provides diffusion times of 0.05 and 0.20 ms for small and big oligomer preparations, respectively. Second, both oligomer batches were brought in contact with lipid vesicles, and changes in the diffusion time of the fluorescently labeled oligomers were observed (black dots). A two-component 3D diffusion model performs the appropriate fitting (shown in black continuous lines, curves 2 and 4) for this scenario: a fast diffusing component corresponding to free (unbound) oligomers and a slow diffusing component corresponding to vesicle bound oligomers. By fixing the fast diffusion time values, known from measurements of oligomers diffusing in solution free of vesicles, we fit for the slow diffusion times and the fractions of bound and free oligomers. To indicate the quality of the fits, the residuals are shown at the top of each panel. In the case of small oligomers (Fig 8A) the shift in diffusion time is obvious. The fraction of bound oligomers (slow component) is >90% and the long diffusion time (~4 ms) indicates vesicle sizes of ~110 nm, in agreement with DLS vesicle size measurements (see Supplemental material). In contrast, in the case of big oligomers produced by *protocol II* (Fig. 8B) the diffusion time shift is minimal due to a very small fraction of bound amyloid oligomers.

An assessment of cell densities (presented in Fig. 9) shows that $A\beta_{1-42}$ oligomers also reduce the numbers of neuronal cells in the cultures: the total number of neurons (viable, necrotic and apoptotic) per sample area in the cultures decreased after treatment with 1 μM $A\beta_{1-42}$ for 24 h. Small oligomers (1–2 nm, *protocol I*) as well as larger oligomers (4–6 nm, *protocol II*) similarly decreased the number of neuronal cells, by 15% and 19%, respectively. While both fractions of oligomers cause a similar reduction of neuron densities in the culture, only the small $A\beta_{1-42}$ aggregates (*protocol I*) caused a significant increase in cell death. In distinction, fibrils had no effect on density of neuronal cells (Fig. 9).

Presence of glial cells may influence the toxicity pattern of $A\beta_{1-42}$. Therefore we additionally tested the effects of Aβ oligomers on CGC cultures treated with cytosine arabinoside (araC) for 10–14 days. After treatment with araC the number of all non-neuronal cells in the cultures was decreased to about 2%. Meanwhile, as shown in Fig. 10, the effects of various forms of $A\beta_{1-42}$ were in principal similar to that observed in glia-rich CGC cultures: small, 2–3 nm oligomers reduced neuronal viability by about 40% compared to control, whereas bigger, 4–6 nm oligomers as well as fibrils and monomers were non-toxic. In distinction from glia-rich CGC, neuronal densities in araC-treated cultures were not affected by $A\beta_{1-42}$: there were 215 ± 10 neurons/field in control, 216 ± 32 in cultures treated with small oligomers, 218 ± 39 in cultures treated with fibrils, and 231 ± 22 in cultures treated with monomers. These data suggest that $A\beta_{1-42}$ oligomers can directly affect neurons

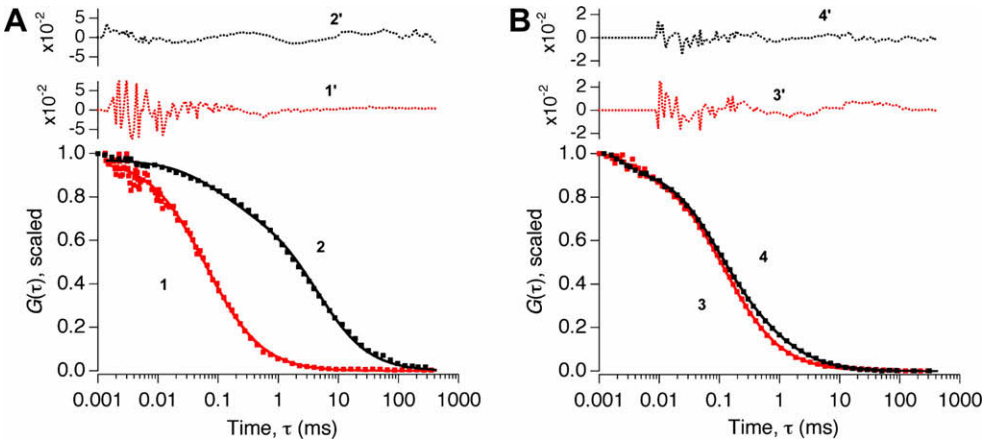

Fig. 8. Different size $A\beta_{1-42}$ oligomers bind differently to lipid membranes. FCS data (dots) are fitted (continuous lines) with a single component 3D diffusion model for fluorescently labeled $A\beta_{1-42}$ diffusing freely in bulk (grey; red in on-line version) and with a two-component 3D diffusion model for $A\beta_{1-42}$ diffusing in the presence of non-fluorescent lipid vesicles (black curves 2 and 4). Residuals of the fits are shown at the top of each panel (curves 1–4). All data are normalized to the same amplitudes of the correlation spectra for comparison. (A) Small $A\beta_{1-42}$ oligomers (*protocol I*), (B) big oligomers (*protocol II*). (For interpretation of the references to color in this figure legend, the reader is referred to the web version of this paper.)

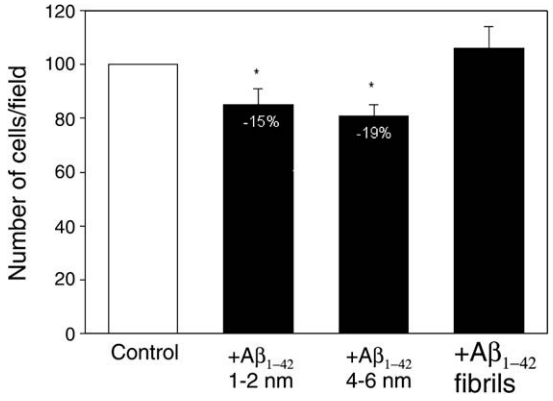

Fig. 9. $A\beta_{1-42}$ oligomers decrease the number of neurons in CGC cultures. After treatment of CGCs with 1 μM of $A\beta_{1-42}$, the total number of viable, necrotic and apoptotic neurons was quantified in 5–7 randomly chosen microscopic fields in each well (two wells per treatment). Total number of cells counted per treatment varied between 1600 and 2500. * – statistically significant effect of $A\beta_{1-42}$ if compared to control. Means ± standard errors of 5–7 separate experiments are presented.

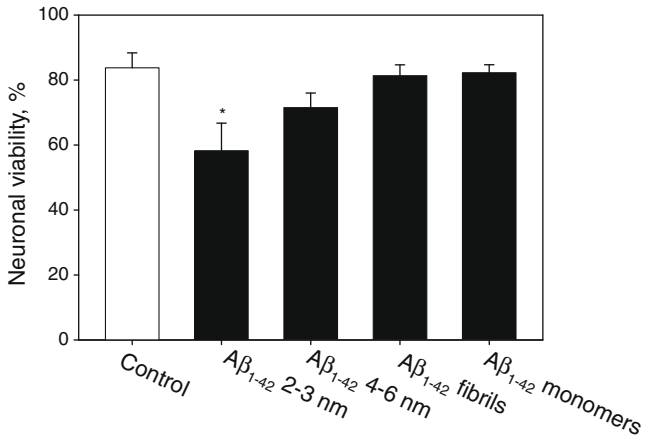

Fig. 10. Effect of $A\beta_{1-42}$ peptides on neuronal cell viability in pure neuronal CGC cultures. CGCs cultures were prepared from 7 to 8 day old Wistar rats as described in Material and methods. Cytosine arabinoside (10 μM) was added within 48 h of plating to prevent glial cell proliferation. Cells were grown *in vitro* for 10–14 days before exposure to $A\beta_{1-42}$. The cultures contained 0.5% microglial cells and 2.1% astrocytes. Cultures were treated with 1 μM of $A\beta_{1-42}$ peptide for 24 h. The viability of neurons in the culture was measured by propidium iodide and Hoechst 33342 staining. * – statistically significant effect of Aβ peptide, if compared to control. Means ± standard errors of four separate experiments are presented.

causing cell death, although a role of glial cells cannot be completely ruled out as these cells may contribute to $A\beta_{1-42}$ neurotoxicity by other indirect mechanism(s).

Discussion

The results of this study show that the most toxic $A\beta_{1-42}$ oligomeric particles are those that exhibit 1–2 nm *z*-heights and circular shape in AFM scans. Assuming the mean density of the protein to be ~1.4 g/cm^3, such 1–2 nm diameter spheres would have a mass that is about the molecular weight of one $A\beta_{1-42}$ monomer. However, both CD and FTIR indicate that the content of α-helix in these particles is minimal (Table 1 and Fig. 6). Because the major secondary structural element of $A\beta_{1-42}$ monomer is the α-helix [22], one can therefore rule out that the toxic preparations of Aβ are dominated by monomers. This raises the question whether the oligomers imaged in Fig. 2A are indeed of spherical shape. The AFM results indicate lateral sizes of several tens of nanometers in the preparations which exhibit *z*-heights from 1 to 2 nm. It is well-known that the apparent size of objects in AFM images is enlarged due to the size of the AFM tip [23]. Especially large distortions occur when the object's size is below the curvature radius of the tip. In our case measured lateral size r_{xy} of the particles with a *z*-height of ~1.5 nm was ~40 ± 3 nm, with r_{xy} depending linearly on *z*. This suggests that the particles shown in Fig. 2A may have true lateral dimensions from 2–3 nm up to 10–15 nm. Therefore, they very likely exhibit lateral dimensions that exceed their *z*-height. The shape of the aggregates may thus deviate significantly from spherical but may more closely resemble oblate spheroids.

This assumption also makes the AFM results consistent with the DLS and FCS analysis. Both techniques determine the diffusion coefficients of oligomers and interpret these in terms of particle geometry under certain assumptions [17]. If the assumption is that the peptide aggregate is spherical, then the Stokes–Einstein equation predicts the size distributions shown in Fig. 3A and B, where the FCS results yield a distribution with an average oligomer diameter of 3.6 nm (average of eight measurements on three different samples), suggesting a considerably bigger size of the particle than

that from the AFM data (Fig. 2). However, if one extends the standard Stokes–Einstein approach to spheroids [24] as described in the Supplemental material, this discrepancy may be resolved. For example, an oblate spheroid with its major and minor axes of ~5 and 1.7 nm (aspect ratio 1:3), respectively, will exhibit about the same diffusion constant as a spherical particle of 3.6 nm diameter. This means that an oblate spheroid imaged by AFM as an object of 1.7 nm *z*-height will exhibit a diffusion constant which under the spherical approximation yields the particle size distribution shown in Fig. 3 with a mean around 3.6 nm. It is noteworthy that in the case of oblate spheroids, the average molecular mass of the aggregates consistent with the FCS results would be more than a factor of two larger than that of ideal spheres. Similarly, the size distribution of *protocol I* oligomers peaks around 2.7 nm (Fig. 3A) in the DLS results, assuming spherical shape of the diffusing particles, but an oblate spheroid with its major and minor axes of 3.8 and 1.9 nm (aspect ratio of 1:2), respectively, would have the same diffusion coefficient. However, the spherical particle would have the molecular weight of ~8 kDa, (consistent with a peptide dimer) while the spheroid would correspond to a molecular mass of ~12 kDa (a peptide trimer). Importantly, these alternate interpretations of the aggregate shapes in the diffusion measurements are consistent with the results of the AFM investigations if one assumes the same deviations from spherical shapes. Taken all together, we suggest that the preparations of oligomeric particles that exhibited high toxicity towards CGCs were populated with $A\beta_{1-42}$ species of low aggregation numbers roughly between dimers and pentamers, with geometric shapes that might be approximated by oblate spheroids.

The FCS data in Fig. 8 show that different size $A\beta_{1-42}$ oligomers bind differently to the phospholipid membrane of vesicles whose composition mimics those of neuronal membranes. While the small oligomers prepared via *protocol I* causes a significant shift of the FCS spectrum towards longer correlation times, the big ones prepared via *protocol II* exhibit just a marginal effect. The increase of the correlation time indicates a slowdown of the thermal motion of the particles that bear the fluorescent label, i.e., amyloid oligomers. The slowing down under the conditions of our experiment may occur only if the fluorescent particle binds to a fluorescently "invisible" vesicle. As evident from the data in Fig. 8A and B, this happens only in oligomer preparations obtained via *protocol I*, which are dominated by the $A\beta_{1-42}$ particles with characteristic *z*-heights from 1 to 2 nm. The marginal change of the FCS spectrum seen in Fig. 8B may be related to the presence of a small amount of low molecular weight oligomer particles in *protocol II* preparations. Alternatively, the shift may be induced by very weak binding of large molecular weight oligomers which would indicate significantly lower binding energy compared to that of the small particles.

Our data demonstrate a striking correlation between the size of $A\beta_{1-42}$ oligomers and their toxicity to neuronal cells. Even though, we did not find any significant differences in the secondary structure of small and bigger $A\beta_{1-42}$ oligomers the cytotoxic effects of these forms were clearly different. Therefore, the main determinant of cytotoxicity seems to be the size of oligomeric $A\beta_{1-42}$ particles. Small oligomeric forms of $A\beta_{1-42}$, with a particle *z*-height of 1–2 nm, similarly as recently observed [25] with N-terminally methionine-substituted amyloid peptide, are the most toxic species and induce rapid necrotic neuronal cell death at low submicromolar concentrations, whereas aggregates above 4–5 nm (oligomers with $n > 14$) do not cause significant cell death. While the cytotoxicity of small (17–22 kDa) oligomers has been known for a decade [26], the continuous transition from highly toxic to non-toxic species as their size increase, is reported here for the first time. On the other hand, even though larger oligomers ($n \approx 12$, MW = 38/48 kDa) were reported [27] to cause full inhibition of the long-term potentiation, our study shows negligible neurotoxicity of particles with >30 kDa (Fig. 6). In contrast to oligomers, $A\beta_{1-42}$ monomers or large fibrillar aggregates were not toxic to CGCs, at least during short time of treatment and at the concentrations used here. These data are consistent with other findings suggesting that oligomeric forms of $A\beta_{1-42}$ can affect neuronal cell cycle events [28], cause impairment of synaptic plasticity and long-term potentiation [7,29], endoplasmic reticulum stress [30] and cell death [9,31]. Dimeric and tetrameric forms of $A\beta_{1-42}$ have been recently shown to be particularly toxic to cortical neurons due to their high binding capacity to lipid membranes [31]. The binding experiment in this work was performed *ex situ*, after the pre-adsorption of the amyloid incubated vesicles onto the hydrophobic surface of the array for the subsequent SELDI-TOF mass-spectroscopy analysis [31]. Our data, in which the amyloid binding to the vesicles was detected *in situ*, strongly supports the idea that the smallest oligomers may be primarily responsible for neurotoxicity observed *in vitro*. In addition, the binding propensity of these species to the phospholipid membrane may differentiate them from the non-toxic oligomer forms.

In most of the studies, the cytotoxic effects of Aβ were observed at higher concentrations (5–10 μM). We show here that the smallest, 1–2 nm oligomeric particles, possibly dimers–pentamers, caused substantial cell death at submicromolar, i.e., pathophysiologically relevant concentrations. Natural $A\beta_{1-42}$ peptide dimers were recently isolated from AD patients brains and were found to cause impairment of synaptic plasticity at nanomolar concentrations [32]. Even though the data in [32] strongly suggest that $A\beta_{1-42}$ dimers may directly target receptors involved in the synaptic transmission, it cannot be ruled out that perturbations of the receptor function may occur through alterations of the physical properties of the phospholipid matrix which accommodates the protein "machinery" of synapses.

Importantly, this study demonstrated that small oligomers of $A\beta_{1-42}$ were toxic to both cerebellar and cortex neurons, whereas glial cells in CGC cultures or macrophage cell lines were resistant to $A\beta_{1-42}$ insult indicating that neuronal cells are particularly sensitive to $A\beta_{1-42}$ oligomers.

Another observation in this study was that bigger (4–5 nm) $A\beta_{1-42}$ oligomer particles caused disappearance of neurons from the treated cultures even without detectable increase in cell death. This suggests that larger oligomers may also be toxic by a different mechanism than $A\beta_{1-42}$ dimers–pentamers. A similar disappearance of neuronal cells has been previously reported by other investigators in mixed neuronal-glial cultures under conditions when microglia were activated, e.g. after treatment of cells with NO, bacterial endotoxins, etc. [13,33]. The causes are unclear at present. One of the likely explanations may be that $A\beta_{1-42}$-affected neurons could be phagocytosed by microglial cells present in mixed CGC cultures. The involvement of microglia in this process is partially supported by our finding that there were no alterations in neuronal densities after incubation with $A\beta_{1-42}$ oligomers in araC-treated cultures. On the other hand, it has been reported [34] that fibrillar Aβ can stimulate phagocytic activity of monocytes and microglia. If oligomeric forms of $A\beta_{1-42}$ have similar effect then it would be possible to speculate that such activated microglial cells may phagocytose Aβ-affected neurons. And if the rate of phagocytosis exceeds the rate by which morphological features of cell death develop, this could result in removal of neurons that did not exhibit apparent signs of cell death. However, a verification of this hypothesis requires more experimental investigations.

Acknowledgments

We thank Dr. Guy Brown for critical reading and comments in the manuscript; Maria Ger for her help with MALDI-TOF spectroscopy; and Justas Barauskas for advising on AFM imaging. This work

was supported by the Lithuanian State Science and Studies Foundation (B38 Amiloide), the NIH (AG032131) and the American Health Assistance Foundation (A2008-307).

Appendix A. Supplementary data

Supplementary data associated with this article can be found, in the online version, at doi:10.1016/j.abb.2010.02.001.

References

[1] J. Hardy, D.J. Selkoe, Science 297 (2002) 353–356.
[2] Y.R. Chen, C.G. Glabe, J. Biol. Chem. 281 (2006) 24414–24422.
[3] C.A. McLean, R.A. Cherny, F.W. Fraser, S.J. Fuller, M.J. Smith, K. Beyreuther, A.I. Bush, C.L. Masters, Ann. Neurol. 46 (1999) 860–866.
[4] J.P. Cleary, Nat. Neurosci. 8 (2005) 79–84.
[5] S. Lesne, M.T. Koh, L. Kotilinek, R. Kayed, C.G. Glabe, A. Yang, M. Gallagher, K.H. Ashe, Nature 440 (2006) 352–357.
[6] P.H. Reddy, M.F. Beal, Trends Mol. Med. 14 (2008) 45–53.
[7] D.M. Walsh, I. Klyubin, J.V. Fadeeva, W.K. Cullen, R. Anwyl, M.S. Wolfe, M.J. Rowan, D.J. Selkoe, Nature 416 (2002) 535–539.
[8] M. Townsend, G.M. Shankar, T. Mehta, D.M. Walsh, D.J. Selkoe, J. Physiol. 572 (2006) 477–492.
[9] R. Resende, E. Ferreiro, C. Pereira, C. Resende De Oliveira, Neuroscience 155 (2008) 725–737.
[10] R. Kayed, Y. Sokolov, B. Edmonds, T.M. McIntire, S.C. Milton, J.E. Hall, C.G. Glabe, J. Biol. Chem. 279 (2004) 46363–46366.
[11] D.M. Walsh, D.J. Selkoe, J. Neurochem. 101 (2007) 1172–1184.
[12] D.M. Hartley, D.M. Walsh, C.P.P. Ye, T. Diehl, S. Vasquez, P.M. Vassilev, D.B. Teplow, D.J. Selkoe, J. Neurosci. 19 (1999) 8876–8884.
[13] A. Bal-Price, G.C. Brown, J. Neurosci. 21 (2001) 6480–6491.
[14] R. Kayed, E. Head, J.L. Thomson, t.M. McIntire, S.C. Milton, C.W. Cotman, C.G. Glabe, Science 300 (2003) 486–489.
[15] G. Valincius, F. Heinrich, R. Budvytyte, D.J. Vanderah, Y. Sokolov, J.E. Hall, M. Loesche, Biophys. J. 95 (2008) 4845–4861.
[16] B. Czarnik-Matusewicz, S. Pilorz, D. Bieńko, D. Michalska, Vib. Spectrosc. 47 (2008) 44–52.
[17] E. Haustein, P. Schwille, Annu. Rev. Biophys. Biomol. Struct. 36 (2007) 151–169.
[18] J.Y. Koh, D.W. Choi, J. Neurosci. Methods 20 (1987) 83–90.
[19] K. Wells, A.A. Farooqui, L. Liss, L.A. Horrocks, Neurochem. Res. 20 (1995) 1329–1333.
[20] W.B.J. Stine, K.N. Dahlgren, G.A. Krafft, M.J. LaDu, J. Biol. Chem. 278 (2003) 11612–11622.
[21] R. Khurana, A.L. Fink, Biophys. J. 78 (2000) 994–1000.
[22] S. Tomaselli, V. Esposito, P. Vangone, N.A.J. van Nuland, A. Bonvin, R. Guerrini, T. Tancredi, P.A. Temussi, D. Picone, ChemBioChem 7 (2006) 257–267.
[23] D.-Q. Yang, Y.-Q. Xiong, Y. Guo, D.-A. Da, W.-G. Lu, J. Mater. Sci. 36 (2001) 263–267.
[24] B. Redouane, P. Robert (Eds.), Soft Matter Characterization, Springer, 2008.
[25] L. Yu, R. Edalji, J.E. Harlan, T.F. Holzman, A.P. Lopez, B. Labkovsky, H. Hillen, S. Barghorn, U. Ebert, Biochemistry 48 (2009) 1870–1877.
[26] M.P. Lambert, K. Barlowa, B.A. Chromy, C. Edwards, R. Freed, R. Liosatos, T.E. Morgan, I. Rozovsky, B. Trommer, K.L. Viola, P. Wals, C. Zhang, C.E. Finch, G.A. Krafft, W.L. Klein, Proc. Natl. Acad. Sci. USA 95 (1998) 6448–6453.
[27] S. Barghorn, V. Nimmrich, A. Striebinger, C. Krantz, P. Keller, B. Janson, M. Bahr, M. Schmidt, R.S. Bitner, J.E. Harlan, A.K. Barlow, U. Ebert, H. Hillen, J. Neurochem. 95 (2005) 834–847.
[28] K. Bhaskar, M. Miller, A. Chludzinski, K. Herrup, M. Zagorski, B.C. Lamb, BMC Mol. Neurodegen. 4 (2009) 14.
[29] I. Klyubin, V. Betts, A.T. Welzel, K. Blennow, H. Zetterberg, A. Wallin, C.A. Lemere, W.K. Cullen, Y. Peng, T. Wisniewski, D.J. Selkoe, R. Anwyl, D.M. Walsh, M.J. Rowan, J. Neurosci. 28 (2008) 4231–4237.
[30] S.M. Chafekar, J.J. Hoozemans, R. Zwart, F. Baas, W. Scheper, Antioxid. Redox Signal. 9 (2007) 2245–2254.
[31] L.W. Hung, G.D. Ciccotosto, E. Giannakis, D.J. Tew, K. Perez, C.L. Masters, R. Cappai, J.D. Wade, K.J. Barnham, J. Neurosci. 28 (2008) 11950–11958.
[32] G.M. Shankar, S. Li, T.H. Mehta, A. Garcia-Munoz, N.E. Shepardson, I. Smith, F.M. Brett, M.A. Farrell, M.J. Rowan, C.A. Lemere, C.M. Regan, D.M. Walsh, B.L. Sabatini, D.J. Selkoe, Nat. Med. 14 (2008) 837–842.
[33] J.J. Neher, G.C. Brown, Biochem. Soc. Trans. 35 (2007) 1166–1167.
[34] B. Wilkinson, J. Koenigsknecht-Talboo, C. Grommes, C.Y. Lee, G. Landreth, J. Biol. Chem. 281 (2006) 20842–20850.